Physica Scripta. Vol. 67, 77–83, 2003

Evolution of a Gas Embedded Z-pinch: A Quasi Static Zero Dimensional Approach

Leopoldo Soto[1,*] and Alejandro Clausse[2,†]

[1] Comisión Chilena de Energía Nuclear, Casilla 188-D, Santiago, Chile
[2] CNEA-CONICET and Universidad Nacional del Centro, 7000 Tandil, Argentina

Received June 11, 2002; accepted September 9, 2002

PACS ref: 52.58.Lq, 52.20.j

Abstract

In gas-embedded Z pinches, high electric discharges are induced in dense gases at atmospheric range pressures. An intriguing phenomenon observed in experiments conducted under these conditions is the radial expansion of the pinch. In this article, a model of Z pinch is derived, which succeeds in explaining expansive Z pinches in terms of variations of the number of particles confined by the pinch. The model is compared with experimental results showing excellent agreement.

1. Introduction

Z pinches are cylindrical plasmas established between two electrodes by means of transient electrical discharges. The axial electric current heats the plasma by Joule effect and simultaneously the Lorentz force compresses the column. Although, MHD instabilities can cause disruption of the discharges, the development of pulse-power generators (delivering currents larger than 10^5 A with $dI/dt > 10^{12}$ A/s) led to the widely held belief that by heating and compressing the plasma at a high enough rate, dense hot plasma conditions could be achieved in times shorter than the instability growth time. It is important to note the renewal interest in Z-pinches research as soft X-ray sources for a thermonuclear inertial confinement device. Under this approach, the Z-pinch is not a dense plasma thermonuclear reactor as it was expected during decades. The pinch provides a very intense soft X-ray source that irradiates a deuterium-tritium target. Active research on Z-pinches is currently ongoing at several laboratories in the USA, England, Germany, Russia and elsewhere. These experiments are carried out in large devices, like at Sandia National Laboratory in the US, in huge generators capable of delivering 20 MA in 100 ns ($dI/dt > 10^{14}$ A/s) into the plasma. This renewed interest is found specifically in fast Z-pinches, and interesting reviews have been published [1,2].

Gas-embedded Z-pinches are produced by discharges in dense gases at near atmospheric pressure, and it corresponds to a kind of quasi-static Z-pinch. As in gas embedded Z-pinches high X-rays or particles beam (neutrons, ions and electrons) have not been measured, the gas embedded Z-pinch is practically not being studied by the Z-pinch community. However, a gas embedded Z-pinch is a useful object for experimental studies of dynamics and stability in pinches. Changing the filling pressure and electrodes configuration, different initial conditions and different stability regimes can be studied. A curious feature observed in the experiments in gas-embedded Z-pinches is the expansion of the pinch [3–5] and an associated increase in the number of ionized particles. This effect (no pinch effect) is rather surprising. Simple zero dimensional models as those presented in references [6,7] assume that the number of ionized particles per unit length (line density) is constant. Those models have been used to describe pinches initiated in fibers. In fiber pinches those models are applied after the fiber has been fully ionized. On the contrary, in gas-embedded Z-pinch experiments, it has been observed that the line density increases as the pinch evolves, indicating that there is a positive input flux of ionized particles into the pinch [3–5, 8–10] and the models described in references [6,7] are not applicable.

In this article, an extended zero dimensional model of a quasi-static Z pinch is derived, which includes the evolution of the number of ionized particles confined by the pinch. The aim of this work relates to the observed radial expansion of the plasma column with the accretion of ionized particles into the plasma using a simple model. The model is compared with a set of experimental data of gas-embedded Z discharges in Hydrogen and Helium at 1/3 atmospheres.

2. Experimental observations

Experiments in gas-embedded Z-pinches were carried out at Pontificia Universidad Católica de Chile [4–5,8–10], using a small pulse power generator, a Marx bank (400 kV) coupled to a water transmission line (1.5 Ω, 300 kV, 120 ns double transit time). The current rate was approximately $2 \cdot 10^{12}$ A/s. The discharges were performed in H_2 and He at 1/3 atmospheres.

Pre-ionization schemes with needle electrodes and continuos micro-discharges lead to stable plasma columns, expanding during the first quarter of the period (~150 ns) of the discharge. On the contrary, applying conventional pre-ionization schemes by pulse laser, the plasma column expands during some 30 ns, until $m = 1$ instabilities transform the plasma cylinder plasma into a helix. A third pre-ionization scheme was also studied, based on a combination of an annular micro-discharge followed by a laser pulse. This scheme produces a double column pinch at the early stage that coalesces into a single plasma column at 60 ns, showing again a period of enhanced stability with no MHD instabilities developing during the current rise

e-mail: lsoto@cchen.cl
e-mail: clausse@exa.unicen.edu.ar

(150 ns). Unfortunately, there are few measurements of the time evolution of the plasma density in this configuration.

The experiments with needle electrodes provide the best experimental data of the expansion phase. The gas was preionized using a small 20 μA discharge induced between two tungsten needle electrodes [4,5]. The electron density profile n, the line electron density N (number of electrons per unit length, $N = 2\pi \int n(r) r \, dr$), and the pinch radius a, were measured with temporal and spatial resolution. A frequency doubled Nd-YAG laser pulse (6 ns) was used for optical diagnostics to obtain multi-frame holographic interferometry (8 frames per discharge, separated from each other by 10 ns) [11], and simultaneous single shot image-plane holographic interferometry and shadowgraphy [5]. The total current and the external voltage were also measured with a Rogowski coil and a capacitive divider.

The results obtained from a series of interferograms in H_2 at 1/3 bar show a plasma column in expansion (Fig. 1). No instabilities were observed during the expansion. An n value of $5 \cdot 10^{25}\,m^{-3}$ is observed at 50 ns at the axis of the pinch, with a value of N of approximately $1.5 \cdot 10^{19}\,m^{-1}$. The Bennett temperature was estimated in $T_B \sim 40$ eV.

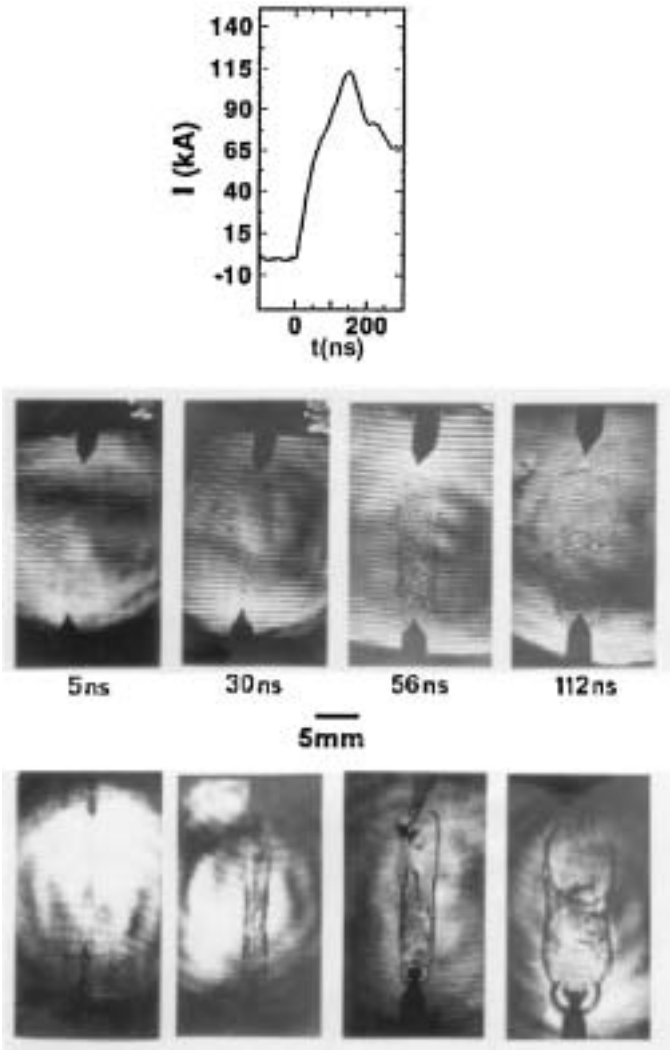

Fig. 1. Experimental observations in discharges operating in hydrogen at 1/3 atmosphere. The figure shows a typical current trace and a simultaneous single shot image-plane holographic interferometry and shadowgraphy.

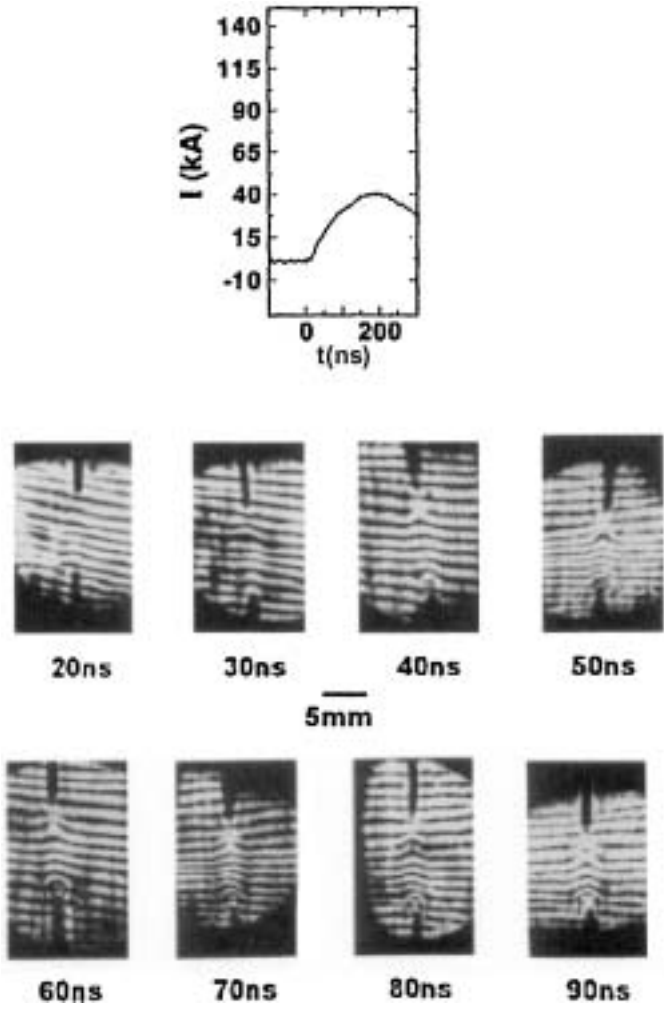

Fig. 2. Experimental observations in discharges operating in helium at 1/3 atmosphere. The figure shows a typical current trace and a sequence of interferograms corresponding to the same discharge. The interferograms were obtained with a multiframe holographic interferometry system (8 frames separated by 10 ns between them per discharge).

The line density, N, increased with a rate of $2.8 \cdot 10^{26}\,m^{-1}\,s^{-1}$ (±30%) and the radial velocity is of the order of $2 \cdot 10^4$ m/s. Details related with the analysis of the interferograms are presented in Appendix I.

The results obtained from multiframe interferograms in He at 1/3 bar (Fig. 2) show that after an initial expansion the pinch radius remains constant from 40 ns to 200 ns. The line density, N, increased with a rate of $7 \cdot 10^{25}\,m^{-1}\,s^{-1}$ (±30%). The observed current and line density and estimated Bennett temperature (no more than 17 eV) are consistent with an ionization state $Z = 1$.

The Alfvén velocity, v_a, for a Z-pinch can be estimated from the measured current I and the line density N [7], and is given by $v_a = 3.88 \cdot 10^9\, I/N^{1/2}$ for H_2 and $v_a = 1.94 \cdot 10^9 I/N^{1/2}$ for He. In both cases the radial velocity is less than the Alfvén velocity, thus the pinch can be considered as quasi-static [4–5,8–10,12].

A general feature is that the pinch tends to expand and the line density N increases. In the next section, a model of a Z-pinch is derived, taking into account this observation. The model will be compared with the experimental results presented above.

3. A lumped parameter model of a Z-pinch

An analytical model, which includes the evolution of the number of ionized particles confined by the pinch, can be constructed for a zero-dimensional description of the quasi-static Z-pinch in terms of the pinch radius a, the number of ions per unit length confined by the pinch (line density N), and the total current I.

A zero-dimensional model means that the radial dependence of the variables (density, temperature and current density) is averaged by integrating across the pinch section, leading to temporal ordinary differential equations of effective lumped variables.

If the radial velocity of the pinch boundary is much less than the Alfvén speed, the evolution of the pinch is quasi-static, and the well-known Bennett relation obtained from pressure equilibrium is applicable. Integrating over the pinch cross section:

$$16\pi NkT = \mu_0 I^2 \tag{1}$$

where k is the Boltzmann's constant and T is the temperature. An homogenous temperature profile $T(r) = T$ has been assumed across the pinch section. However, it is important to note that the Bennett relation stands independently of the shape of the ions density, n, and current density J. Thus, Eq. (1) essentially gives the average temperature for a given line density N and for a given total current I.

The energy equation can be written as:

$$\frac{\partial u}{\partial t} + \frac{1}{r}\frac{\partial}{\partial r}(ruv) + \frac{p}{r}\frac{\partial}{\partial r}(rv) + \frac{1}{r}\frac{\partial}{\partial r}(rq) = \frac{J^2}{\sigma} - L \tag{2}$$

with $u = p/(\gamma - 1)$ denoting the specific internal energy per unit volume, $p = 2nkT$ the pressure, γ the specific heat ratio, v the radial velocity, q the radial heat flux, J the axial current density, σ the electrical conductivity. The terms in the right-hand side are the ohmic power input, and the energy loss L. The nomenclature is also listed in Table I.

Table I. *Parameters used in the model.*

Nomenclature	
a	Pinch radius
I	Current
I_{PB}	Pease–Braginski current limit
J	Current density
k	Boltzmann constant
n	electron density = ion density
N	Number of ions per unit volume = Number of electrons per unit volume
p	Pressure
q	Radial heat flux
r	Radial coordinate
R	Radiation loss
L	Term of losses in the energy equation
s	Ion source
T	Temperature
t	Time
u	Specific internal energy per unit volume, $u = p/(\gamma - 1)$
u_i	Ionization potential
v	Radial velocity
$\alpha_\perp$	Plasma transversal Spitzer conductivity coefficient, $1618\,\mathrm{s\,A^2/Jm\,eV^{3/2}}$
γ	Specific heat ratio, $\gamma = 5/3$
μ_o	Vacuum permeability, $4\pi 10^{-7}\,\mathrm{J/mA^2}$
σ	Conductivity
ξ	Shape factor

In order to include the time evolution of the number of particles confined by the pinch, the continuity equation must be used carefully. Three different situations are considered:

(a) *Surface ionization at zero temperature*. It is assumed that the ionization is produced in the edge of the plasma column ($r = a$) and the ionized particles are incorporated to the plasma at zero temperature. Thus, the continuity equation is written as:

$$\frac{\partial n}{\partial t} + \frac{1}{r}\frac{\partial}{\partial r}(nrv) = 0 \tag{3}$$

with the following boundary conditions,

$$2\pi rnv|_{r=a} = -\frac{\mathrm{d}N}{\mathrm{d}t},$$

$$2\pi rq|_{r=a} = u_i\frac{\mathrm{d}N}{\mathrm{d}t},$$

$$2\pi ruv|_{r=a} = 0. \tag{4}$$

In Eqs. (4), u_i is the ionization potential.

(b) *Surface ionization at temperature T*. It is assumed that the ionization is produced at the edge of the plasma column ($r = a$) and the ionized particles are incorporated to the plasma at the same plasma temperature $T(T_e = T_i = T)$. The continuity equation corresponds to Eq. (3), with the followings boundary conditions,

$$2\pi rnv|_{r=a} = -\frac{\mathrm{d}N}{\mathrm{d}t},$$

$$2\pi rq|_{r=a} = (u_i + 3kT)\frac{\mathrm{d}N}{\mathrm{d}t},$$

$$2\pi ruv|_{r=a} = -3kT\frac{\mathrm{d}N}{\mathrm{d}t}. \tag{5}$$

(c) *Volumetric ionization*. An isolated pinch is assumed, with ionization in bulk of the plasma volume. The continuity equation is now:

$$\frac{\partial n}{\partial t} + \frac{1}{r} + \frac{\partial}{\partial r}\,(nrv) = s \tag{6}$$

with the followings boundary conditions,

$$2\pi rnv|_{r=a} = 2\pi rq|_{r=a} = 2\pi ruv|_{r=a} = 0 \tag{7}$$

and the ion source, s, satisfies:

$$\int_0^a 2\pi rs\,\mathrm{d}r = \frac{\mathrm{d}N}{\mathrm{d}t}. \tag{8}$$

In the cases in which surface ionization was assumed, (a) and (b), the energy loss is due to Bremsstrahlung radiation R, thus $L = R = \beta_B n^2 T^{1/2}$, with β_B denoting the Bremsstrahlung coefficient. On the other hand, in the case in which volumetric ionization is assumed the losses include Bremsstrahlung radiation and the energy necessary to ionize the new particles incorporated to the plasma, thus $L = R + u_i s$.

In order to average Eq. (2) over the pinch volume, let us assume uniform temperature distribution, and that the velocity varies linearly with r, that is:

$$av = r\frac{\mathrm{d}a}{\mathrm{d}t}. \tag{9}$$

Relation (9) is exact for processes in the region of self-similar solutions.

It has been shown [6,7] that the radiated power is related to the Ohmic heating power by:

$$\int 2\pi r R \,\mathrm{d}r = \frac{1}{\pi r^2 \sigma}\frac{I^4}{I_{PB}^2} \tag{10}$$

where I_{PB} is the Pease–Braginskii current, and the classical Spitzer conductivity σ is given by:

$$\sigma = \alpha_\perp T^{3/2}. \tag{11}$$

Considering that $u = 2nkT/(\gamma - 1)$, with $\gamma = 5/3$ and $Z = 1$, Eq. (2) can be integrated over the pinch cross section, leading to:

$$\frac{3\mu_o}{8\pi} I\frac{\mathrm{d}I}{\mathrm{d}t} + \frac{\mu_O}{4\pi}\frac{I^2}{a}\frac{\mathrm{d}a}{\mathrm{d}t} = \frac{\xi}{\pi\alpha_\perp}\left(\frac{16\pi k}{\mu_o}\right)^{3/2}\left(1 - \frac{I^2}{I_{PB}^2}\right) \times \frac{N^{3/2}}{Ia^2} - u_i\frac{\mathrm{d}N}{\mathrm{d}t}, \tag{12}$$

where ξ is a shape factor for the distribution of n and J ($\xi = 1$ corresponds to a flat current and a parabolic ion density). Note that Eq. (12) is obtained using any of the ionization models (a), (b) or (c).

Equation (12) relates the evolution of three important variables of the pinch: the current, I, the linear ion density, N, and the external radius, a, which were measured in the experiments cited in this paper. The fact that the three different assumptions for the continuity equations with the corresponding boundary conditions give the same result (Eq. (12)) is not surprising since the model is zero-D and should be independent of the radial structure.

The measured line density variation $N(t)$ are shown in Figs. 3 and 4. Assuming a fully ionized hydrogen plasma, these data can be introduced in Eq. (12) in order to compare the temporal evolutions of the pinch radius. Equation (12) was numerically solved using the LSODE FORTRAN solver package. The curve in Fig. 3 is the theoretical evolution of the pinch radius predicted by Eq. (12) showing an excellent agreement with the experimental observations. The points correspond to experimental data obtained from the interferograms shown in Fig. 1. The only parameter that was numerically determined in Eq. (12) was the shape factor ξ, which resulted in 0.24 for hydrogen.

On the other hand, the experiments in helium gas showed that the plasma was not fully ionized in that case. The observed current and line density, and the Bennett temperature estimation (no more than 17 eV), are consistent with an ionization state $Z = 1$. However, Eq. (12) considers a Spitzer conductivity for a fully ionized plasma, and therefore a direct application of the model in helium is questionable. Keeping this warning in mind, Eq. (12) was applied to the helium data (Figs. 2 and 4). The shape factor

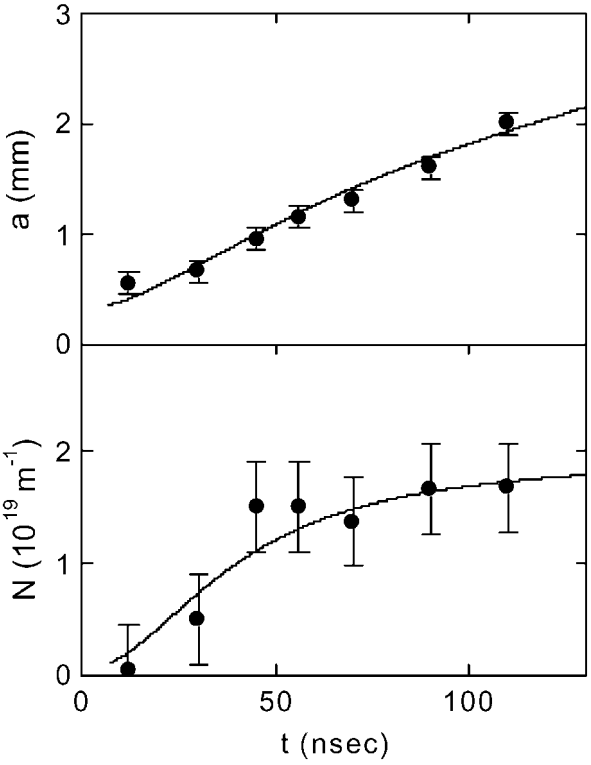

Fig. 3. Linear ion density and pinch radius in a discharge in 1/3 atmosphere of H_2. ($u_i = 15$ eV, $\xi = 0.24$). The points correspond to experimental data obtained from interferograms as those shown in Fig. 1.

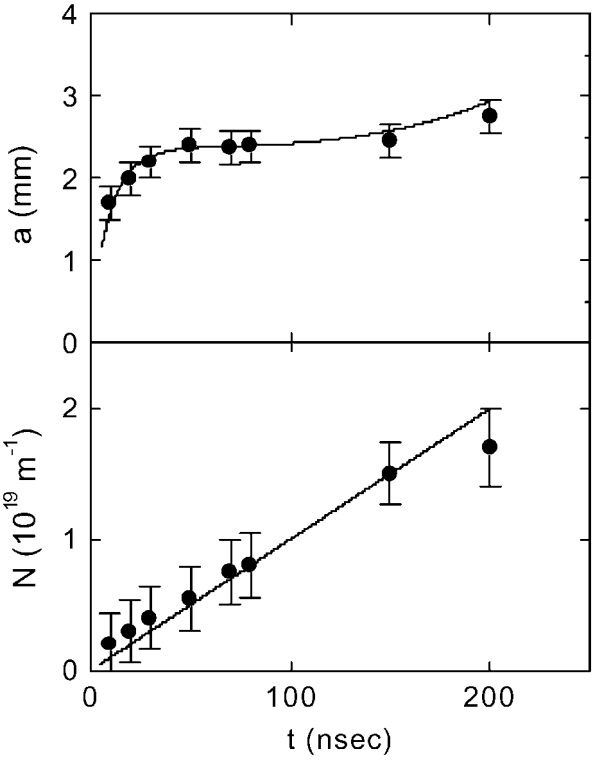

Fig. 4. Linear ion density and pinch radius in a discharge in 1/3 atmosphere of He. ($u_i = 24$ eV, $\xi = 0.52$). The points correspond to experimental data obtained from interferograms as those shown in Fig. 2. The curve $a(t)$ is the theoretical evolution of the pinch radius predicted by Eq. (12).

ξ resulted in a value 0.52 for helium. In spite of the theoretical questions, good agreement was found, which can be explained taking into account that the partially

ionized plasma conductivity coefficient is roughly absorbed into the effective parameter ξ.

4. Discussions and Conclusions

A zero dimensional model for the time evolution of the quasi-static Z-pinch was developed. This model introduces plasma line density temporal variations, being an extension of a previous zero dimensional model in which the line density was assumed constant [6,7]. For constant line density, the present model reduces to the Haines–Robson model [6,7].

The model was compared with experimental measurements in gas-embedded Z-pinches showing a good agreement (Figs. 3 and 4). The radial expansion observed experimentally in gas embedded Z-pinches is explained by the increment of ionized particles in the plasma.

The stability of the plasma column has been discussed in Refs. [5,9,10,12] and is beyond the scope of this paper. More sophisticated calculations using one-dimensional two-temperature MHD equations [13] account for the accretion of ionized particles into the plasma, and show that the structure of the initially pre-ionized region greatly affects the pinch dynamics and the internal pinch structure, in accordance with the experiments described above. In the present model, the effect of the internal structure of the pinch is lumped in a shape parameter, which represents the degree of departure from uniform J and parabolic n radial profiles. For instance, in the case of a "hollow" current profile which increases linearly with radius as $J = J_0 \times (1 + a/r)$ for $r < a$, and $J = 0$ for $r > a$, along with the corresponding ion density profile n for pressure balance, the shape factor ξ achieves a value of the order of 0.5. It is worth noting that there is an infinite number of combinations of $J(r)$ and $n(r)$ that produce the same ξ value. Therefore, we cannot determine the current and ion density profiles from the values of ξ that arise from the experimental values shown in Figs. 3 and 4. Taking into account that there are no experimental measurements of the current profile J in gas-embedded Z-pinches, it is reasonable to include a shape factor to describe quasi-static Z-pinch dynamics with a zero-D model. The simple model presented here captures the essential physics observed in gas embedded Z-pinches with radial expansion associated with increasing number of ions in the pinch.

The model presented here is not closed (the number of ions per unit length is extracted from the experimental data and not from the model itself). Physical mechanisms for the ionization rate should be included in order to calculate the number of ionized particles per unit length, as for example diffusion of particles from the neutral gas as was suggested in Ref. [3]. Also other physical mechanisms, as those studied in relation to channel sparks by S. I. Braginskii in the fifties [14], should be considered in order to close the model.

A gas embedded Z-pinch is a useful object for experimental studies of dynamics and stability in pinches. Changing the filling pressure and electrodes configuration, different initial conditions and different stability regimes can be studied. A closed zero-D model would be a useful tool to assist in the design of experimental conditions and electrode configurations. Experiments operating at mega-Ampere currents are being planned to be performed using the SPEED 2 device [15,16] (now at the Comisión Chilena de Energía Nuclear, Chile) with a double column pre-ionization scheme [8], where enhanced stability and compression have been observed in contrast with conventional pre-ionization schemes [9,10].

Acknowledgements

The authors acknowledge the fruitful discussions with: M. G. Haines and M. Coppins of Imperial College, UK; H. Chuaqui and M. Favre of Pontificia Universidad Católica de Chile; H. Bruzzone of Universidad de Mar del Plata (Argentina) and M. Skowronek of France.

This work has been funded by the grant *Cátedra Presidencial en Ciencias*, awarded to L. Soto by the Chilean Government, CCHEN 573, and the Chilean–Argentinean Project on Innovative Applications of Thermonuclear Fusion.

Appendix I. Calculation of the number of particles per unit length from the interferograms

The number of particles per unit length was determined from the electron density profile calculated from the fringe deviation of the interferograms by means of an Abel inversion, this is the method most widely known and used. On the other hand, the line density was also determined directly from the fringe deviation as will be shown in Eq. (A-12).

Determination of the line density by means of the Abel inversion

The plasma refraction index is given by [17]:

$$\mu = 1 + \sum_i K_i n_i \tag{A-1}$$

with K_i denoting the refractivity of the different plasma components and n_i its density.

The refraction index due the electrons μ_e, is:

$$\mu_e = 1 - \frac{e^2 \lambda n}{2\pi m_e c^2} \tag{A-2}$$

where e and m_e are the electron charge and mass, c is the light speed, λ the wavelength of the beam probe and n the electron density. In SI units:

$$\mu_e - 1 = -4.49 \cdot 10^{-16} \lambda^2 n. \tag{A-3}$$

In Eq. (A-2) and (A-3) the angular frequency of the light beam is assumed to be much larger than the frequency of the electron-ion collision, the frequency of the electron-neutral collision, the cyclotron frequency of the electrons and the plasma frequency.

The refraction index due to the neutral components of the plasma, μ_n, is obtained from the Cauchy dispersion formula [17]. If the light frequency is much larger than the resonant line frequency of the atom, the refraction index due the neutral components is

$$\mu_n - 1 \cong \left(A + \frac{B}{\lambda^2} \right) \frac{n_n}{n_L}. \tag{A-4}$$

Here n_n is the density of the neutral atoms, n_L is the Loschmidt number ($n_L = 2.69 \cdot 10^{25}\,\mathrm{m}^{-3}$) and the density of the background gas, n_o, is $n_o = p n_L$, (with p denoting the pressure). For the visible region of the spectrum, the

constants A and B satisfy $B/\lambda^2 \ll A$, and the refractivity of the atoms and molecules is rather independent of wavelength. The Cauchy formula is valid if the distance between the wavelength of the beam probe λ and the wavelength of the absorption lines is greater than the width of the corresponding absorption line.

Using Eq. (A-4), the refraction index due to neutral particles of H_2 is:

$$\mu_n - 1 = 2.99 \cdot 10^{-30} n_n \quad (n_n \text{ in SI units}). \tag{A-5}$$

In addition, the refraction index of the background gas for H_2 at 1/3 atmosphere is:.

$$\mu_o - 1 = 1.368 \cdot 10^{-4} p \quad (p \text{ in atmospheres}). \tag{A-6}$$

For the Nd-YAG laser wavelength ($\lambda = 532\,\text{nm}$) the electron refractive index is given by

$$\mu_e - 1 = -1.27 \cdot 10^{-28} n \quad (n \text{ in SI units}). \tag{A-7}$$

Note that electron and neutrals produce opposite fringe deviation.

Figure A-1 shows a typical fringe shift profile observed in an interferogram (note that S is dimensionless). The fringe shift is related to the pinch coordinate y. The fringe shift at a point y in the figure is given by,

$$S(y) = \frac{1}{\lambda} \int_{L(y)} [(\mu_e - 1) + (\mu_n - 1) + (\mu_o - 1)]\, \mathrm{d}l. \tag{A-8}$$

The axial symmetry observed in the interferograms indicates that n and n_n depend only on the pinch radius, thus

$$S(y) = \frac{2}{\lambda} \int_{|y|}^{\rho} \frac{(\mu - 1)}{(r^2 - y^2)^{1/2}} r\, \mathrm{d}r \tag{A-9}$$

with ρ denoting the total radius ($\rho = a_n$ in Fig. A-1). Equation (A-9) is an Abel integral equation, whose solution is an Abel inversion,

$$\mu - 1 = \frac{-\lambda}{\pi} \int_r^{\rho} \frac{\mathrm{d}S(x, y)/\mathrm{d}y}{(y^2 - r^2)^{1/2}}\, \mathrm{d}y. \tag{A-10}$$

Equation (A-10) can be solved numerically using Eqs. (A-5), (A-6) and (A-7), and assuming that the electron and neutral density distributions do not overlap. The latter is based on the fact that the fringe shifts at the edge and at the inside of the pinch have opposite signs, and that the fringe shift due to electrons is greater than the fringe shift due to neutrals. The calculation starts at the edge a_n and proceeds towards the axis. The pinch radius is considered at a. The portion of S between a and a_n corresponds to the high-density neutral layer. Figure A-2 shows a density profile obtained from the fringe shown in Fig. A-1. The error in n increases towards the axis. The error on the axis was estimated in 20%. It is important to note that in practice the electrons and neutrals overlap close to the defined pinch radius a. The value of n and n_n at the pinch border, a, are much lower than the respective maximum values. Therefore, neutral particles can be ionized and incorporated into the pinch, and consequently Eqs. (1) to (4) are valid in gas embedded Z-pinches. In order to obtain the overlapped profiles at the boundary of the pinch two-wavelength interferometry must be used as diagnostics.

The line density, N, is defined by the integral of the electron density over the pinch section A,

$$N = \int\int_A n(x, y)\, \mathrm{d}x\, \mathrm{d}y = 2\pi \int_0^a n(r) r\, \mathrm{d}r. \tag{A-11}$$

For the electron density profile shown in fig. A-2, N equals $1.11 \cdot 10^{19}\,\text{m}^{-1}$.

Determination of the line density directly from the fringe shift

On the other hand, the line density can also be determined directly from the fringe deviation, realizing that in Eq. (A-12) S is proportional to $\int n\, \mathrm{d}x$, whereby:

$$\begin{aligned} N &= \int\int_A n(x, y)\, \mathrm{d}x\, \mathrm{d}y = \int \left(\int n\, \mathrm{d}x \right) \mathrm{d}y \\ &= \int \left(\frac{1}{4.49 \cdot 10^{-16} \lambda} S \right) \mathrm{d}y \\ &= 4.19 \cdot 10^{21} \int_{-a}^{a} S\, \mathrm{d}y \quad (\text{in SI units}). \end{aligned} \tag{A-12}$$

This method is more direct and therefore have lower errors than the Abel inversion. Using Eq. (A-12) for the fringe deviation shown in Fig. A-1, N equals $1.17 \cdot 10^{19}\,\text{m}^{-1}$.

For each interferogram, three fringes were used to obtain N, one at the middle of the electrodes, a second between the middle and the cathode, and the third between the middle and the anode. The line density was determined by averaging the values calculated with each method over all the fringes.

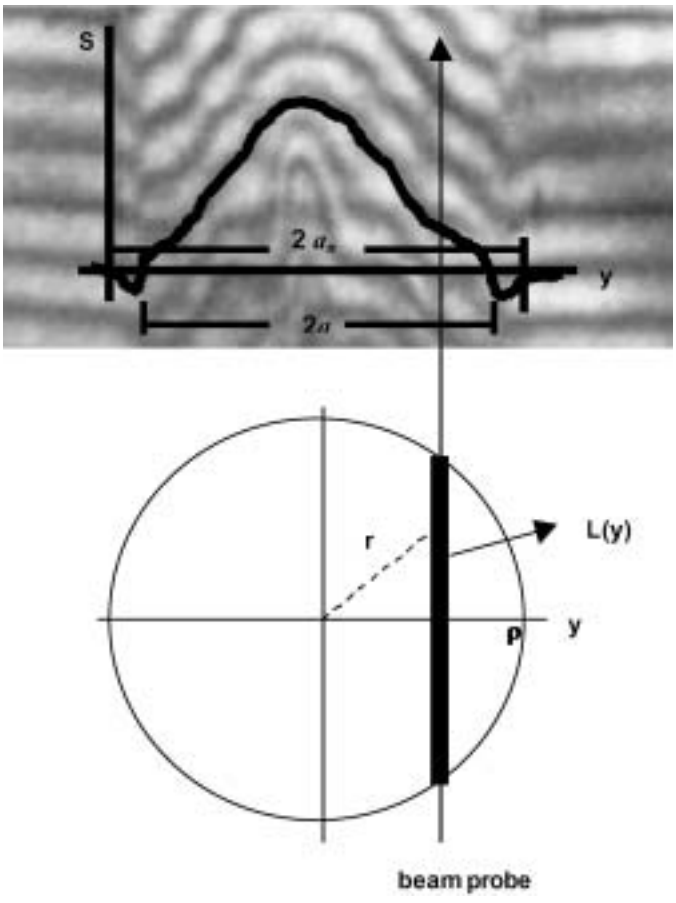

Fig. A-1. Typical fringe shift profile observed in interferograms and cross section (in x-y plane) of the plasma column. The detailed portion is from the interferogram corresponding to 56 ns in Fig. 1.

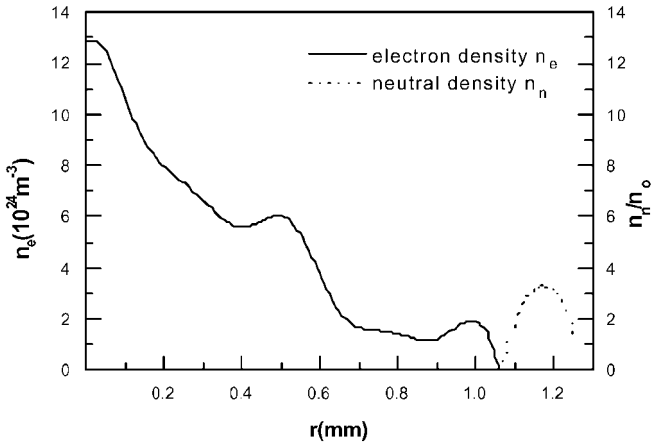

Fig. A-2. Electron and neutral density profiles obtained from the fringe shift shown in Fig. A-1. The neutrals are normalized to the background, H_2 at 1/3 atmosphere, i.e. $n_o = 1.79 \cdot 10^{25}$ m^{-3}.

References

1. Ryutov, D. D., Derzon, M. S. and Matzen, M. K., Rev. Mod. Phys. **72**, 167 (2000).
2. Liberman, M. A., De Groot, J. S., Toor, A. and Spielman, R. B., "Physics of High-Density Pinch," (Springer-Verlag, 1998).
3. Choi, P., Coppins, M., Dangor, A. E. and Favre, M. B., Nucl. Fusion **28**, 1771 (1988).
4. Soto, L., "Dinámica de un Z-pinch. Experimentos en fondo de gas neutro", Ph.D. dissertation, Pontificia Universidad Católica de Chile, Santiago de Chile (1993).
5. Chuaqui, H., Soto, L., Favre, M. and Wyndham, E., "Parameter space comparison with universal diagram for Z-pinch stability", in Proc. 3rd Int. Conf. Dense Z-Pinches (London, UK, 1993), AIP Conf. Proc. (ed. M. Haines) (American Institute of Physics, Melville, NY, 1993), p. 27.
6. Robson, A. E., Nucl. Fusion **28**, 2171 (1988).
7. Haines, M. G., Plasma Phys. Control. Fusion **31**, 759 (1989).
8. Soto, L., Chuaqui, H., Favre, M. and Wyndham, E., Phys. Rev. Lett. **72**, 2891 (1994).
9. Soto, L. *et al.*, IEEE Trans. Plasma Sci. **24**, 1162 (1998).
10. Soto, L., Chuaqui, H., Favre, M. and Wyndham, E., "Gas embedded compressional Z-pinch experiments", in Proc. Int. Conf. on Plasma Phys. ICPP, 1994, Foz do Iguazú, Brazil, (1994), p. 216.
11. Soto, L., Chuaqui, H. and Skowronek, M., Appl. Opt., **34**, 7831 (1995).
12. Soto, L. *et al.*, Phys. Plasmas **8**, 2572 (2001).
13. Esaulov, A., Sasorov, P., Soto, L. and Zambra, M., Phys. Plasmas **8**, 1395 (2001).
14. Braginskii, S. I., Soviet Physics JETP **34**, 1068 (1958).
15. Decker, G., Kies, W., Mälzig, M., Van Valker, C. and Ziethen, G., Nucl. Instrum. Meth. **A249**, 477 (1986).
16. Soto, L. *et al.*, Brazilian J. Phys. **32**, 139 (2002).
17. Ostrovsky, Yu. I., Butusov, M. M. and Ostrovskaya, G. V. "Interferometry by Holography", (Springer-Verlag, 1980).